Supplementary information

Carrier generation and compensation mechanism in $La_2SnO_2S_3$

Teruya Nagafuji,[a] Koshiro Osuna,[a] Kota Hanzawa,[a] Tomoya Gake,[a] Soungmin Bae,[a] Zhongxu Hu,[b] Takayoshi Katase,[b] Akira Takahashi,[a] Hidenori Hiramatsu,[*ab] and Fumiyasu Oba [**ab]

[a] Laboratory for Materials and Structures, Institute of Innovative Research, Tokyo Institute of Technology, 4259 Nagatsuta, Midori-ku, Yokohama 226-8501, Japan

[b] MDX Research Center for Element Strategy, International Research Frontiers Initiative, Tokyo Institute of Technology, 4259 Nagatsuta, Midori-ku, Yokohama 226-8501, Japan

[*] Email: h-hirama@mces.titech.ac.jp

[**] Email: oba@msl.titech.ac.jp

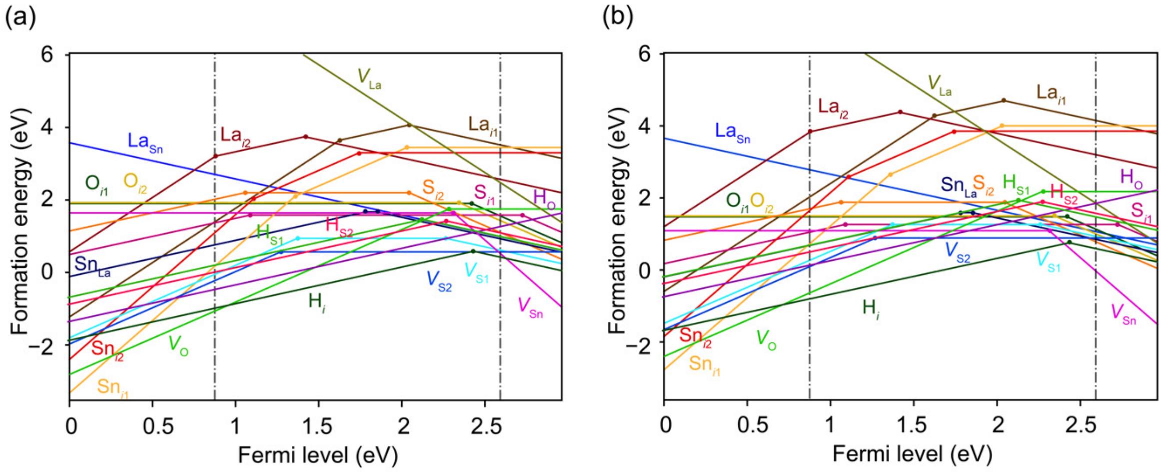

Fig. S1 Formation energies of native defects and H impurities at relevant sites in $La_2SnO_2S_3$ under (a) the cation-rich conditions [$\Delta\mu_{La} = -5.17$, $\Delta\mu_{Sn} = -0.64$, $\Delta\mu_{O} = -2.76$, $\Delta\mu_{S} = -0.37$, and $\Delta\mu_{H} = 0$ (eV)] and (b) the anion-rich conditions [$\Delta\mu_{La} = -5.80$, $\Delta\mu_{Sn} = -1.19$, $\Delta\mu_{O} = -2.33$, $\Delta\mu_{S} = -0.05$, and $\Delta\mu_{H} = -0.16$ (eV)], calculated using PBEsol. The upper and lower limits of the Fermi level are expanded from the band edges within the 2×2×1 non-Γ-centered *k*-point mesh used in the PBEsol supercell calculation (the vertical dashed-dotted lines) to those determined by the non-self-consistent HSE (α = 0.31) band structure calculation; the Fock-exchange mixing parameter α has been tuned to reproduce the band gap by the self-consistent HSE06 (α = 0.25) calculation.

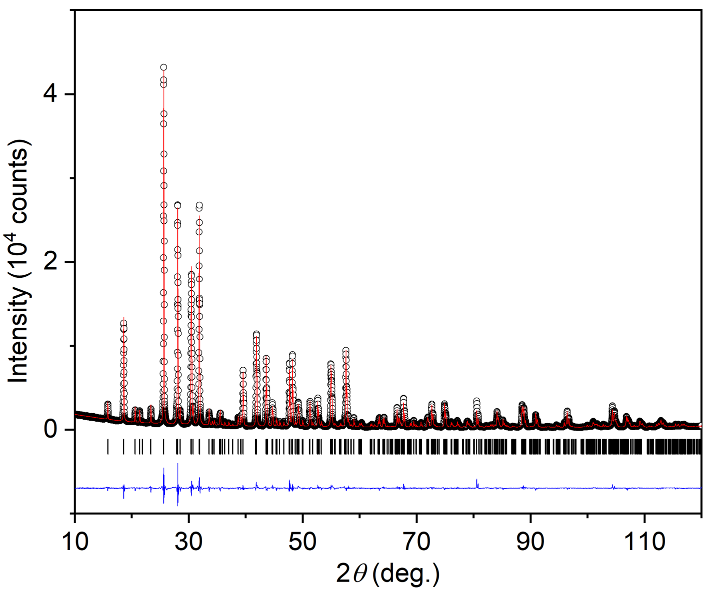

Fig. S2 Results of Rietveld analysis of a polycrystalline $La_2SnO_2S_3$ sample. The black circles, red curve, black bars, and blue curve denote the original data points, fitted curve, diffraction peak positions, and difference between the original data points and the fitted curve, respectively.

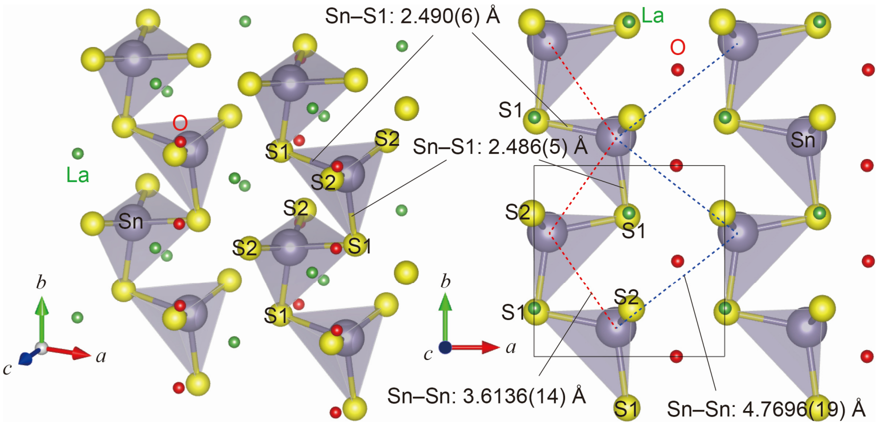

Fig. S3 Crystal structure of $La_2SnO_2S_3$ drawn from two kinds of viewpoints. La (green) and O (red) are represented in smaller diameters than those in Fig. 9 to clearly show the SnS_4 tetrahedra. The red and blue dotted lines show the first and second neighboring Sn–Sn distances, respectively. The VESTA code[55] was used for the visualization.

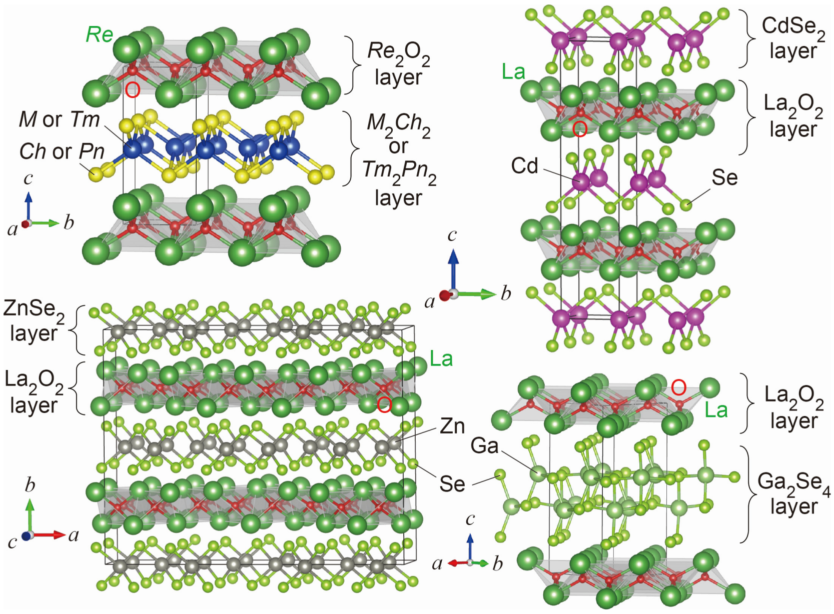

Fig. S4 Crystal structures of *ReMOCh* (*Re* = rare earth, La–Er; *M* = monovalent metal, Cu, Ag; *Ch* = chalcogen, S–Te), *ReTmOPn* (*Re* = La–Sm; *Tm* = 3d or 4d transition metal, Cr–Ni, Zn, Ru, Os; *Pn* = pnictogen, P–Sb), $La_2CdO_2Se_2$, $La_2ZnO_2Se_2$, and $LaGaOSe_2$. All of these layered quaternary mixed-anion compounds possess a common building block of an edge-sharing rare-earth oxide Re_2O_2 tetrahedra layer, which is sandwiched by chalcogenide or pnictide layers. The VESTA code[55] was used for the visualization.

Table S1 Values of the chemical potentials and the competing phases at each limit of the single-phase region of $La_2SnO_2S_3$ in the La–Sn–O–S–H quinary system from HSE06 hybrid functional calculations.

Conditions	$\Delta\mu_{La}$ (eV)	$\Delta\mu_{O}$ (eV)	$\Delta\mu_{S}$ (eV)	$\Delta\mu_{Sn}$ (eV)	$\Delta\mu_{H}$ (eV)	Competing phases
A*	−5.25	−2.90	−0.52	−0.32	0	H_2, La_2S_3, La_2SO_2, SnS
B	−5.27	−2.89	−0.51	−0.33	0	H_2, La_2S_3, La_2SnS_5, SnS
C	−5.67	−2.62	−0.39	−0.45	−0.02	H_2O, H_2S, SnS, SnS_2
D	−5.44	−2.81	−0.42	−0.42	0	H_2, H_2S, La_2SnS_5, SnS
E	−5.40	−2.80	−0.42	−0.51	0	H_2, H_2S, La_2S_3, La_2SO_2
F	−5.40	−2.81	−0.42	−0.50	0	H_2, H_2S, La_2S_3, La_2SnS_5
G	−5.54	−2.65	−0.42	−0.51	0	H_2, H_2O, H_2S, La_2SO_2
H	−5.59	−2.65	−0.42	−0.42	0	H_2, H_2O, H_2S, SnS
I	−5.49	−2.65	−0.52	−0.32	0	H_2, H_2O, La_2SO_2, SnS
J**	−6.15	−2.32	0	−1.22	−0.21	H_2S, La_2SO_6, LaS_2, S, SnS_2
K	−5.91	−2.51	−0.12	−0.98	−0.15	H_2S, La_2SnS_5, LaS_2, SnS_2
L	−6.01	−2.36	−0.07	−1.22	−0.18	H_2S, La_2SO_2, La_2SO_6, LaS_2, LaSO
M	−5.77	−2.54	−0.19	−0.98	−0.12	H_2S, $La_{10}S_{19}$, La_2SO_2, LaS_2
N	−5.77	−2.57	−0.19	−0.91	−0.12	H_2S, $La_{10}S_{19}$, La_2SnS_5, LaS_2
O	−5.51	−2.77	−0.39	−0.45	−0.02	H_2S, La_2SnS_5, SnS, SnS_2
P	−5.89	−2.36	−0.32	−0.73	−0.15	H_2O, La_2SO_2, La_2SO_6, $La_2Sn_2O_7$
Q	−6.02	−2.32	−0.26	−0.71	−0.16	H_2O, La_2SO_6, $La_2Sn_2O_7$, SnS_2
R	−5.99	−2.36	−0.13	−1.11	−0.15	H_2O, H_2S, La_2SO_2, La_2SO_6
S	−6.10	−2.32	−0.09	−1.04	−0.16	H_2O, H_2S, La_2SO_6, SnS_2
T	−5.65	−2.63	−0.26	−0.85	−0.08	H_2S, $La_{10}S_{19}$, La_2S_3, La_2SO_2
U	−5.65	−2.64	−0.26	−0.83	−0.08	H_2S, $La_{10}S_{19}$, La_2S_3, La_2SnS_5
V	−5.58	−2.56	−0.52	−0.32	−0.05	H_2O, La_2SO_2, $La_2Sn_2O_7$, SnS
W	−5.83	−2.45	−0.39	−0.45	−0.10	H_2O, $La_2Sn_2O_7$, SnS, SnS_2

* The cation-rich conditions.

** The anion-rich conditions.

Table S2 Values of the chemical potentials and the competing phases at each limit of the single-phase region of $La_2SnO_2S_3$ in the La–Sn–O–S quaternary system from HSE06 hybrid functional calculations.

Conditions	$\Delta\mu_{La}$ (eV)	$\Delta\mu_{O}$ (eV)	$\Delta\mu_{S}$ (eV)	$\Delta\mu_{Sn}$ (eV)	Competing phases
A	−5.27	−2.89	−0.51	−0.33	La_2S_3, La_2SnS_5, SnS
B	−5.65	−2.64	−0.26	−0.83	$La_{10}S_{19}$, La_2S_3, La_2SnS_5
C	−5.51	−2.77	−0.39	−0.45	La_2SnS_5, SnS, SnS_2
D	−5.77	−2.57	−0.19	−0.91	$La_{10}S_{19}$, La_2SnS_5, LaS_2
E	−5.91	−2.51	−0.12	−0.98	La_2SnS_5, LaS_2, SnS_2
F*	−6.15	−2.32	0	−1.22	La_2SO_6, LaS_2, S, SnS_2
G	−6.14	−2.32	0	−1.22	La_2SO_6, LaS_2, SnS_2
H	−5.65	−2.63	−0.26	−0.85	$La_{10}S_{19}$, La_2S_3, La_2SO_2
I	−5.77	−2.54	−0.19	−0.98	$La_{10}S_{19}$, La_2SO_2, LaS_2
J	−6.01	−2.36	−0.07	−1.22	La_2SO_2, La_2SO_6, LaS_2, LaSO
K**	−5.25	−2.90	−0.52	−0.32	La_2S_3, La_2SO_2, SnS
L	−5.58	−2.56	−0.52	−0.32	La_2SO_2, $La_2Sn_2O_7$, SnS
M	−5.89	−2.36	−0.32	−0.73	La_2SO_2, La_2SO_6, $La_2Sn_2O_7$
N	−5.83	−2.45	−0.39	−0.45	$La_2Sn_2O_7$, SnS, SnS_2
O	−6.02	−2.32	−0.26	−0.71	La_2SO_6, $La_2Sn_2O_7$, SnS_2

* The anion-rich conditions.

** The cation-rich conditions.

Table S3 Thermodynamic transition levels ε(*q*/*q*') of the selected native defects and the H interstitial in reference to the VBM from HSE06 hybrid functional calculations.

	q/*q*'	ε(*q*/*q*') (eV)
Sn_{i1}	4+/2+	1.15
	2+/0	1.66
Sn_{i2}	4+/2+	0.81
	2+/0	1.63
V_O	2+/0	2.16
	0/2−	2.60
V_{S1}	2+/0	0.98
	0/2−	2.24
V_{S2}	2+/0	1.02
	0/2−	2.56
V_{Sn}	0/2−	1.91
	2−/4−	1.98
H_i	+/−	2.41

Table S4 Lattice parameters determined by WPPF (Whole Powder Pattern Fitting) analysis and reliability (*R*)-factors obtained by Rietveld refinements for $La_2SnO_2S_3$. Values in the parentheses of lattice parameters are standard deviations in the last digit.

Chemical formula	$La_2SnO_2S_3$
Crystal system	Orthorhombic
Space group	*Pbnm* (No. 62)
Refined 2θ region (deg.)	10 – 120
a (Å)	5.86215(17)
b (Å)	5.87512(17)
c (Å)	19.0666(5)
R_{wp} (%)	6.35
R_p (%)	4.69
S	1.95

Table S5 Refined structure parameters for $La_2SnO_2S_3$. Values in parentheses are standard deviations in the last digit.

Atom	Site	Occupancy	*x*	*y*	*z*	*B* (Å^2)
La	8*d*	1.00	0.00225(15)	0.25221(11)	0.06368(2)	0.024(10)
Sn	4*c*	1.00	0.4295(2)	0.1523(2)	1/4	0.99(2)
O	8*d*	1.00	0.2467(12)	0.4992(15)	–0.0002(4)	0.15(10)
S1	4*c*	1.00	0.0125(10)	0.2332(8)	1/4	0.77(3)
S2	8*d*	1.00	0.5117(6)	0.2509(5)	0.13536(9)	0.77(3)

Table S6 Summary of structure parameters for SnS_2, SnS, and $La_2SnO_2S_3$.

Formula	SnS_2	SnS		$La_2SnO_2S_3$	
Structure type	CdI_2	GeS		–	
Space group	$P\bar{3}m1$ (No. 164)	*Pnma* (No. 62)		*Pbnm* (No. 62)	
Crystal system	Trigonal	Orthorhombic		Orthorhombic	
Formal charge of Sn	+4	+2		+4	
Coordination number of Sn	6	3	6	4	6
Connectivity of Sn polyhedra	Edge sharing (‖ *a*, *b*)	Corner sharing (‖ *b*, *c*)	Edge sharing (‖ *b*, *c*)	Corner sharing (‖ *b*)	Edge sharing (‖ *ab*)
Sn–S (Å)	2.5601(11)×6	2.622(3)×1 2.6618(19)×2	2.622(3)×1 2.6618(19)×2 3.287(3)×2 3.385(3)×1	Sn–S2: 2.312(2)×2 Sn–S1: 2.486(5)×1 (‖*ab*) Sn–S1: 2.490(6)×1 (‖*ab*)	Sn–S2: 2.312(2)×2 Sn–S1: 2.486(5)×1 (‖*ab*) Sn–S1: 2.490(6)×1 (‖*ab*) Sn–S1: 3.430(5)×1 (‖*ab*) Sn–S1: 3.451(6)×1 (‖*ab*)
Bond valence sum (BVS) of Sn	3.9	1.6	1.9	4.1	4.2
S–Sn–S (deg.)	89.20(5)×6 90.80(5)×6 180.0000(0)×3	89.02(6)×2 96.83(9)×1	89.02(6)×2 96.83(9)×1 76.71(6)×2 79.11(7)×2 117.01(5)×2 92.78(6)×2 74.55(7)×1 162.66(8)×2 161.98(4)×1	S1–Sn–S2: 99.02(10)×2 S1–Sn–S2: 102.69(9)×2 S1–Sn–S1: 108.87(17)×1 (‖*ab*) S2–Sn–S2: 141.96(17)×1	S1–Sn–S2: 99.02(10)×2 S1–Sn–S2: 102.69(9)×2 S1–Sn–S1: 108.87(17)×1 (‖*ab*) S2–Sn–S2: 141.96(17)×1 S1–Sn–S2: 74.34(8)×2 S1–Sn–S2: 76.06(10)×2 S1–Sn–S1: 76.39(14)×1 (‖*ab*) S1–Sn–S1: 84.69(18)×1 (‖*ab*) S1–Sn–S1: 90.06(14)×1 (‖*ab*) S1–Sn–S1: 161.08(19)×1 (‖*ab*) S1–Sn–S1: 166.4(3)×1 (‖*ab*)
Sn–Sn (Å)	3.6456(5) (‖ *a*, *b*) 5.8934(12) (‖ *c*)	3.4867(16) 3.982(3) (‖ *b*) 4.1450(17) 4.329(3) (‖ *c*)		3.6136(14) (‖ *ab*) 4.7696(19) (‖ *ab*) 9.7350(6) (≅‖ *c*) 10.0396(4) (≅‖ *c*)	
S–S (Å)	3.595(3)×6 (≅‖ *c*) 3.6456(5)×6 (‖ *ab*) 3.647(3) (≅‖ *c*)	3.704(3)×4 3.891(5)×2 3.982(3)×2 4.329(3)×2 5.690(5)×2		S1–S2: 3.581(5)×2 S1–S2: 3.654(6)×2 S1–S2: 3.662(6)×2 S1–S2: 3.748(5)×2 S1–S1: 4.048(9)×2 (‖ *ab*) S2–S2: 4.054(5)×1 (‖ *ab*) S1–S1: 4.255(9)×2 (‖ *ab*) S2–S2: 4.248(6)×1 (‖ *ab*)	
O–La (Å)	–	–		2.375(8)×1 2.393(8)×1 2.421(8)×1 2.427(8)×1	
La–O–La (deg.)	–	–		104.4(3)×1 104.5(4)×1 104.8(4)×1 105.3(3)×1 118.9(4)×1 119.7(4)×1	
La–S (Å)	–	–		3.184(4)×1 3.234(3)×1 3.248(3)×1 3.284(4)×1	
S–La–S (deg.)	–	–		78.14(9)×1 78.34(9)×1 81.12(9)×1 81.33(9)×1 129.99(6)×1 130.02(6)×1	
Reference	53 (ICSD Collection Code 252197)	54 (ICSD Collection Code 24376)		This work	